

RESEARCH ARTICLE

Metal–Organic Framework-Based Ultrafast Logic Gates for High-Security Optical Encryption

Junhong Yu^{1,2}, Yadong Han^{1,2}, Longyu Wang¹, Yibing Liu¹, Hang Zhang^{1,2}, Xuan Chen³, Xuezhi Liu³, Zhengbang Wang^{3*}, and Jianbo Hu^{1,2*}

¹Laboratory for Shock Wave and Detonation Physics, Institute of Fluid Physics, China Academy of Engineering Physics, Mianyang 621900, China. ²State Key Laboratory for Environment-Friendly Energy Materials, Southwest University of Science and Technology, Mianyang 621010, China. ³Key Laboratory for the Green Preparation and Application of Functional Materials Ministry of Education, Hubei Key Laboratory of Polymer Materials, School of Materials Science and Engineering, Hubei University, Wuhan 430062, China.

*Address correspondence to: jianbo.hu@caep.cn (J.H.); zhengbang.wang@hubei.edu.cn (Z.W.)

Optical logic gates call for materials with giant optical nonlinearity to break the current performance bottleneck. Metal–organic frameworks (MOFs) provide an intriguing route to achieve superior optical nonlinearity benefitting from structural diversity and design flexibility. However, the potential of MOFs for optoelectronics has been largely overlooked and their applications in optical logic have not been exploited. Here, through temporally manipulating the nonlinear optical absorption process in porphyrin-based MOFs, we have successfully developed AND and XOR logic gates with an ultrafast speed approaching 1 THz and an on–off ratio above 90%. On this basis, all-optical information encryption is further demonstrated using transmittance as primary codes, which shows vast prospects in avoiding the disclosure of security information. To the best of our knowledge, this is the first exploration of MOFs for applications in ultrafast optical logic devices and information encryption.

Introduction

Integrated circuits that utilize networked logic gates to process Boolean logic operations are building blocks of modern computation and information processing [1,2]. Unfortunately, current electronic transistor-based logic gates are approaching their final performance limitations (i.e., reaching the ending of Moore's law [3]) due to impractical energy consumption [4] and restricted operation speed [5]. In contrast to electronic logic gates, the all-optical logic gate [1,6], a fundamentally new technology that operates by optical nonlinearity and utilizes photons as information carriers, offers an unprecedented opportunity to circumvent the “electric bottleneck” [7] and satisfy the growing demand in computational processing power nowadays. However, the majority of proposed designs [8–11] to realize optical logics have yet to show improved performance compared to their current electronic counterparts. One of the essential challenges is that tiny optical nonlinearity in materials imposes general trade-offs between speed, energy, footprint, and dissipation [6,10].

To circumvent the abovementioned challenge and improve the nonlinearity from the matter part, recent intriguing ideas have smartly utilized metal–organic frameworks (MOFs) as matrices to host molecules with strong intrinsic optical nonlinearity

[12,13]. Benefitting from the structural diversity [14] and coordinately orientated organic molecules [15], photo-induced carrier absorption and relaxation processes in such systems can be flexibly controlled [16], therefore providing the possibility to exhibit giant optical nonlinearity [17,18]. Furthermore, with the development of MOF synthesis methods, the highly structured and crystalline surface-supported MOF nanofilms (SURMOFs) [12,19] make this material even more promising for optical logic devices. Unfortunately, current application-oriented MOF studies have focused on electrochemistry/catalysis [20,21] and the giant optical nonlinearity in MOFs has never been exploited for optical logic gates so far.

In this work, we have demonstrated that by using femto-second laser pulse sequences, porphyrin-based SURMOFs can be used as a material platform for ultrafast optical logic gates based on the physics of nonlinear optical absorption processes (i.e., a phenomenon in which the absorption process differs under low and high optical excitation [22]). Our strategy changes the dynamic competition among different absorption processes by injecting an additional nonequilibrium carrier population from the control pulse, thereby permitting an ultrafast and deep modulation of the probe pulse transmittance (e.g., an on–off ratio of more than 90% and a switching speed faster than 1 ps have been achieved for the proposed AND

Citation: Yu J, Han Y, Wang L, Liu Y, Zhang H, Chen X, Liu X, Wang Z, Hu J. Metal–Organic Framework-Based Ultrafast Logic Gates for High-Security Optical Encryption. *Ultrafast Sci.* 2023;3:Article 0030. <https://doi.org/10.34133/ultrafastscience.0030>

Submitted 28 December 2022
Accepted 16 April 2023
Published 12 May 2023

Copyright © 2023 Junhong Yu et al. Exclusive licensee Xi'an Institute of Optics and Precision Mechanics. No claim to original U.S. Government Works. Distributed under a Creative Commons Attribution License (CC BY 4.0).

and XOR logic gates). More importantly, as a proof-of-concept logic implementation of the proposed optical gates, we have further achieved high-security information encryption and authentication using probe transmittance as primary codes. These results have provided new application scenarios for MOFs and will stimulate fascinating MOF-based photonic applications.

Methods

OA, Z-scan measurements

The barium boron oxide (BBO) crystal is utilized to double the output of a Ti:sapphire amplifier (1 kHz, 45 fs, 800 nm, Spectra-Physics) into a 400-nm, 100-fs laser pulse. The laser pulse with a wavelength of 400 nm is incident onto the porphyrin MOF nanofilm with a Plano-convex spherical lens (focal length = 150 mm), and the beam size at the focal spot is about $\sim 12.5 \mu\text{m}$ in radius. The porphyrin MOF nanofilm is mounted on the linear delay stage to change the beam size excited on the sample, and transmittance is measured by the lock-in system (SR830, Stanford Research Systems).

Probe-control experiments

The output of a Ti:sapphire laser (center wavelength: $\sim 800 \text{ nm}$; pulse width: $\sim 45 \text{ fs}$) is frequency-doubled into 400 nm using the BBO crystal and then split into 2 beams with a 1:1 intensity ratio, which is used as the control and probe pulses, respectively. A scan delay unit in the probe arm is used to control the time separation (Δt) between the control and probe pulses. The polarization of the control pulses is perpendicular to the probe pulse to avoid any optical interference, and these 2

sequential optical pulses are focused on the sample fixed at the focal plane.

Results

Porphyrin-based SURMOFs on quartz substrates are synthesized based on the so-called liquid phase epitaxy to form self-assembly of cobalt ions and porphyrin molecules [[5,10,15,20-(4-carboxyphenyl) porphyrin] (TCPP)] [12,15]. As schematically illustrated in Fig. 1A, the porphyrin-SURMOF is based on the established SURMOF-2 structure with 2 building units [23]: Co-oxo trinuclear clusters are connected with ditopic TCPP linkers to yield a packed 3-dimensional topological network with highly oriented chromophores (the infrared absorption spectrum has confirmed the formation of coordination bonds between TCPP and Co acetates based on the vanishment of the C=O stretching in the free carboxylic group of TCPP; see details in Fig. S1). Meanwhile, the scanning electron microscopy image presented in Fig. S2 indicates a highly uniform nanofilm with a thickness of 400 nm and distinct in-plane/out-of-plane peaks in x-ray diffraction verify that porphyrin-based SURMOFs are orientated along the [011] lattice direction (see Fig. S3) [12,15,23]. Furthermore, absorption and photoluminescence spectra (see Fig. S4) inform that the Soret band, which corresponds to the transition from the ground state (S_0) to the second excited state (S_2), is located around 420 nm. To characterize whether porphyrin-based SURMOFs are suitable for optical logic gates, the optical nonlinearity is measured in situ by the open-aperture (OA), Z-scan technique with the 400-nm, 100-fs pulse excitation (details of the Z-scan

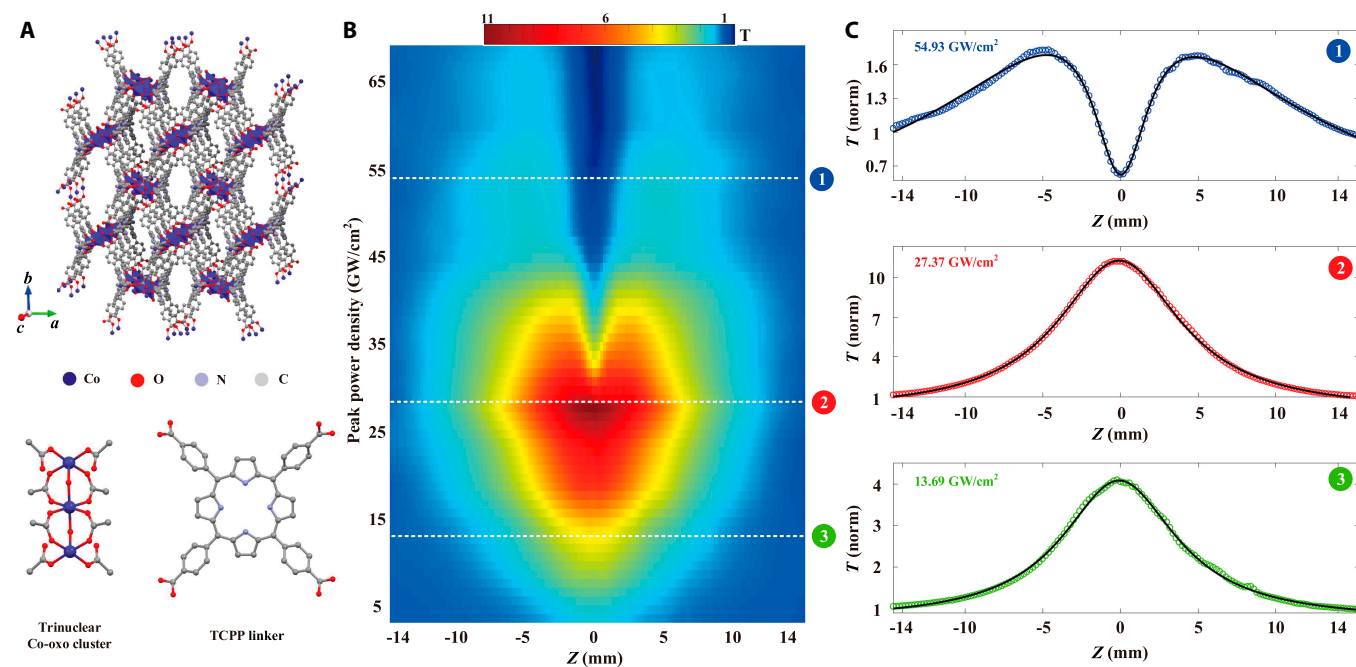


Fig. 1. Excitation density-dependent OA Z-scan measurements of porphyrin-based SURMOFs. (A) Schematic diagram of the structure of porphyrin SURMOFs, which are the self-assembling of cobalt ions and porphyrin linkers. (B) The 2-dimensional map of 400-nm laser pulse transmittances as a function of the scan distance and the excitation peak density, in which a clear transition from SA to RSA with increasing excitation densities can be observed. Please note that the measured optical transmittance is normalized based on the value when the sample is far away from the focal point [i.e., $\text{abs}(Z) = 15 \text{ mm}$]. (C) Transmittance curves with 3 representative excitation intensities are presented. Black curves are fitted with the nonlinear transmission equation.

experiment are provided in Methods). The normalized excitation intensity-dependent optical transmittances are presented in Fig. 1B (individual Z-scan curves with different excitation intensities can be found in Fig. S5), which clearly exhibits that the transmittance of porphyrin-based SURMOFs is distinct with increasing excitation densities (I): With I less than 27.37 GW/cm^2 , the highest transmittance is found at the focal point, which suggests the saturable absorption (SA), while with I above 27.37 GW/cm^2 , a typical characteristic of reverse saturable absorption (RSA) gradually appears with a transmittance valley near the focal point.

The dramatic transition from SA to RSA in a narrow excitation intensity range, together with the strong SA response (i.e., the normalized transmittance in the SA regime is as high as 11), indicates that porphyrin-based SURMOFs should

exhibit a giant nonlinear optical absorption process. To quantitatively determine the nonlinear absorption coefficient, the nonlinear transmission equation is utilized to fit the Z-scan trace [24–26]:

$$T(z) = \frac{1}{\sqrt{\pi}q} \int_{-\infty}^{+\infty} \ln[1 + q \exp(-t^2)] dt \quad (1)$$

where $q = \beta \times I_0 \times L_{\text{eff}} / (1 + z^2/z_0^2)$, with β being the third-order nonlinear absorption coefficient, I_0 being the excitation density at the focal point, and z_0 being the Rayleigh length, and the effective sample thickness L_{eff} is linked to the linear absorption coefficient (α) and the sample thickness (L) by $L_{\text{eff}} = [1 - \exp(-\alpha L)]/\alpha$. The fitting results (see the black curves in Fig. 1C) show that β is as high as $2.64 \times 10^{-3} \text{ cm/W}$, which

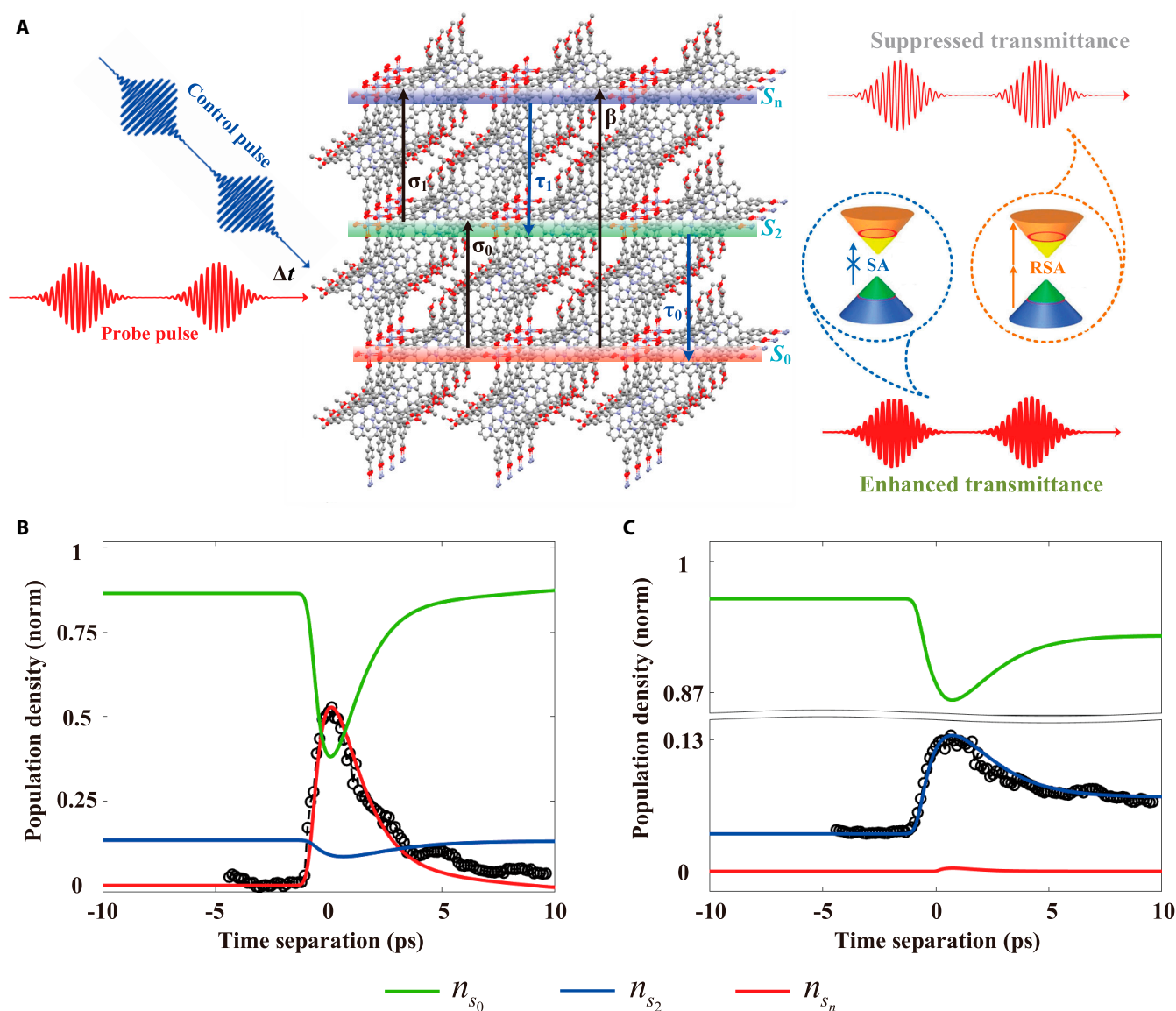


Fig. 2. Ultrafast modulation of the optical transmittance based on the pump-probe configuration. (A) Schematic illustration of the operation principle with the sample fixed at the focal plane. By adjusting the time ordering (Δt) and excitation intensity of the control and probe pulse, the probe transmittance will be enhanced or suppressed according to the dynamic competition between the absorption processes. The 3-energy diagram and the corresponding dynamic processes are also presented. (B) Kinetic simulation of the normalized population density in different states with varying time separations (Δt) for the suppressed transmittance. (C) Kinetic simulation of the normalized population density in different states with varying time separations (Δt) for enhanced transmittance. The black circles in (B) and (C) are the rescaling experimental data presented in Fig. 3C and F, which show good agreement with the theoretical result.

exhibits great potential in nonlinear optics (for comparison, β at 400 nm in graphene [27], black phosphorus [28], metal chalcogenides [29], and MXenes [30] is typically smaller than 1×10^{-3} cm/W).

According to the electronic state distribution in porphyrin-based SURMOFs [12,31], one-photon absorption (OPA; S_0 to S_2), excited-state absorption (ESA; S_2 to S_n), and two-photon absorption (TPA; S_0 to S_n) occur with the highest transition probability under the 400-nm excitation. Therefore, the nonlinear absorption-induced SA to RSA transition can be described by the 3-energy diagram (see Fig. 2A). Please note that the triplet level contribution to the nonlinear absorption has been neglected due to the slower intersystem crossing compared to the femtosecond pulse excitation [32]. It can be seen that with different excitation intensities, the transmittance variation in porphyrin-based SURMOFs is governed by these 3 absorption processes (i.e., OPA, ESA, and TPA) and the intensity transmitted through the sample can be determined by [26,33] $dI/dz \propto -[\sigma_0 n_{s_0} + \sigma_1 n_{s_2} + \beta I]I$ (where σ_0 and σ_1 are the one-photon and excited-state absorption coefficient, respectively; n is the population density in the corresponding energy level). Therefore, it is natural to expect that if the excitation is separated in the time domain (i.e., 2 pulse excitations with different time ordering), the nonequilibrium carrier distribution will substantially change the dynamic competition among these 3 absorption processes, resulting in an ultrafast modulation of light transmittance. Following this thought, Fig. 2A shows the operation principle of all-optical transmittance switching based on a probe-control configuration. Here, the probe pulse propagating through the sample located at the focal plane serves as signal input/output, while the control pulse with a time separation (Δt) is utilized to change the dynamic competition among OPA, ESA, and TPA processes.

Before moving on to the experimental realization, the proposed optical modulation concept is theoretically examined in our kinetic simulations [11,34,35] based on the 3-level energy diagram (full details are given in Note S1 and Figs. S6 to S7). Please note that this kinetic model utilizes 2 Gaussian excitation pulses (I_{probe} and I_{control}) with a time separation (Δt) to mimic the probe-control configuration and the probe pulse excitation intensity is always in the regime of SA. Let us first consider suppression of the probe transmittance: When the control pulse is strong enough (i.e., $I_{\text{probe}} + I_{\text{control}} > 27.37$ GW/cm²), TPA and ESA processes will overwhelm the OPA process, manifesting as a dominated occupation of the S_n state shown in Fig. 2B. Consequently, the probe transmittance will be greatly suppressed because of the SA to RSA transition. It is worth mentioning that since the S_n population density at $\Delta t < 0$ (i.e., the control pulse arrives later than the probe pulse) is simply determined by the ESA/TPA process, the probe transmittance modulation speed is faster than 1 ps, while for $\Delta t > 0$ (i.e., the control pulse arrives earlier than the probe pulse), dynamics of carriers excited by the control pulse entangle with the probe pulse absorption process, which thus slows down the modulation speed [7,36]. On the other hand, if a weak control pulse is adopted (i.e., $I_{\text{probe}} + I_{\text{control}} \leq 27.37$ GW/cm²), OPA still dominates the absorption process with a negligible S_n population density (see Fig. 2C) and, as a result, the probe pulse transmittance modulation mainly arises from occupation changes in the S_2 state and an enhanced response is expected due to the Pauli blocking principle [29,30,33].

Closely following the concept discussed in Fig. 2, we have designed an all-optical XOR logical gate based on the probe-control configuration, in which the incident control and probe pulses serve as 2 inputs and the pulse propagated through the sample is the output terminal (more details of the experimental implementation are provided in Methods). As listed in the truth table (see Fig. 3A), with $I_{\text{probe}} = I_{\text{control}} = 27.37$ GW/cm², when the probe pulse is on (logical state 1) and the control pulse is off (logical state 0), the probe transmittance of ~ 11 will not be influenced and the output is positive (logical state 1); however, if both control and probe pulses are on (logical state 1), the probe transmittance will be greatly suppressed due to the RSA process and the output becomes negative (logical state 0). To determine the modulation depth, we have checked the probe transmittance with and without the control pulse incident in a zero time delay. As shown in Fig. 3B, the presence of the control pulse can decrease the probe transmittance to ~ 0.7 , corresponding to an on/off ratio above 90% [37]. More importantly, this significant modulation can be reversibly tuned by switching on and off the control pulse excitation and the output signal remains nearly unchanged after several 10 min, which demonstrates good reproducibility and low material fatigue [38].

Another qualitative criterion of logical gates is the modulation speed, which can be determined by varying time separations (Δt) between control and probe pulses. Fig. 3C displays a representative time evolution of the probe transmittance, revealing an ultrafast response with $\Delta t < 0$ that vanishes within a ~ 0.72 ps period and a much slower response when $\Delta t > 0$, as deduced from an exponential decay fit convoluting with the laser cross-correlation function [39,40]. With rescaling the probe transmittance dynamics, a nice agreement is achieved with the simulated S_n population density in Fig. 2B, which confirms again our interpretation of the switching behavior: An ultrafast response with $\Delta t < 0$ arises purely from the TPA and ESA, which can modify the probe transmittance in a virtually instantaneous manner and allows the modulation speed above 1 THz, while if the control pulse arrives earlier than the probe pulse ($\Delta t > 0$), the ultrafast nature is lost due to the involvement of relatively slow photocarrier relaxation dynamics, which results in a biexponential recovery process with a short lifetime of ~ 0.75 ps and a long lifetime of ~ 17.4 ps. Please note that this slow lifetime is consistent with the carrier deexcitation process (~ 22.3 ps, from S_2 to S_0) in porphyrin-based SURMOFs (see the measured carrier dynamics in Fig. S8).

Aside from the XOR gate, an all-optical AND logic gate (see Fig. 3D) is also demonstrated using $I_{\text{probe}} = I_{\text{control}} = 13.69$ GW/cm², in which with 2 inputs on (logical state 1), the probe transmittance is still in the SA regime and will be largely enhanced due to the Pauli blocking; thus, a positive output is obtained (logical state 1). Similarly, we have also determined the modulation depth and speed of the AND gate. As shown in Fig. 3E, an on/off ratio of $\sim 60\%$ is achieved with and without the control pulse modulation, which also exhibits a stable performance during a reasonably long time duration. Regarding the modulation speed, we can understand that the probe transmittance recovery process with $\Delta t < 0$ in the AND gate is slower than that in the XOR gate due to negligible contributions from TPA and ESA processes under weaker excitation conditions, as observed in Fig. 3F. It is worth mentioning that when Δt is negative, a sharp response has still been resolved with a lifetime of ~ 1.28 ps due to the giant linear absorption coefficient of porphyrin MOFs at 400 nm ($49,860$ cm⁻¹) [12]. Moreover, a

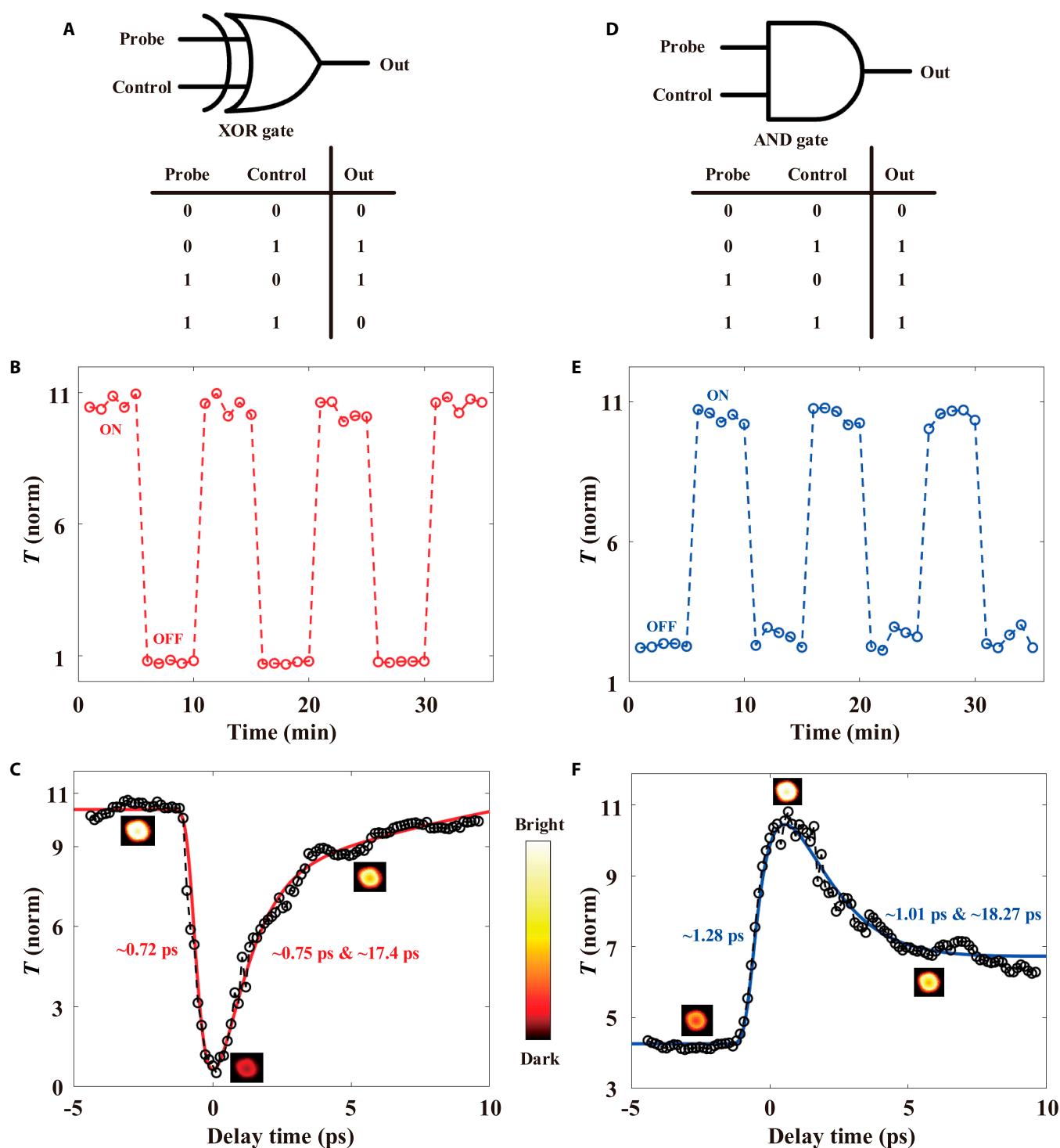


Fig. 3. Ultrafast XOR and AND logic gates. (A and D) Schematic of XOR and AND logic gates. (B and E) The normalized probe transmittance of XOR and AND gates by switching on and off the control pulse excitation in a zero-time separation fashion ($\Delta t = 0$). (C and F) Time evolutions of the probe transmittance change as a function of time separations between the control and probe pulses. Insets: Intensity images of the probe spot at 3 representative time separations. Black circles are measured data, while blue and red curves are the exponential fitting convoluted with a Gaussian instrument response function ($SD \sigma = 100$ fs).

good consistency between the rescaling experimental data and the simulated S_2 population density is observed (see Fig. 2C), which confirms again that occupation changes in the S_2 state govern the probe transmittance modulation in the AND gate.

As a proof-of-concept logic operation of the proposed all-optical MOF-based gates, we have demonstrated a novel and

high-security information encryption system with the probe transmittance (T) as cryptographic primitives. As shown in Fig. 4A, we set an encoding rule of “00” for $T = T_0 < T_{\max}$, “01” for $T_0 < T < T_{\max}$, “10” for $T_0 < T = T_{\max}$, and “11” for $T < T_0 < T_{\max}$. Here, T_0 denotes the probe transmittance without the control pulse modulation and T_{\max} represents the maximum probe transmittance

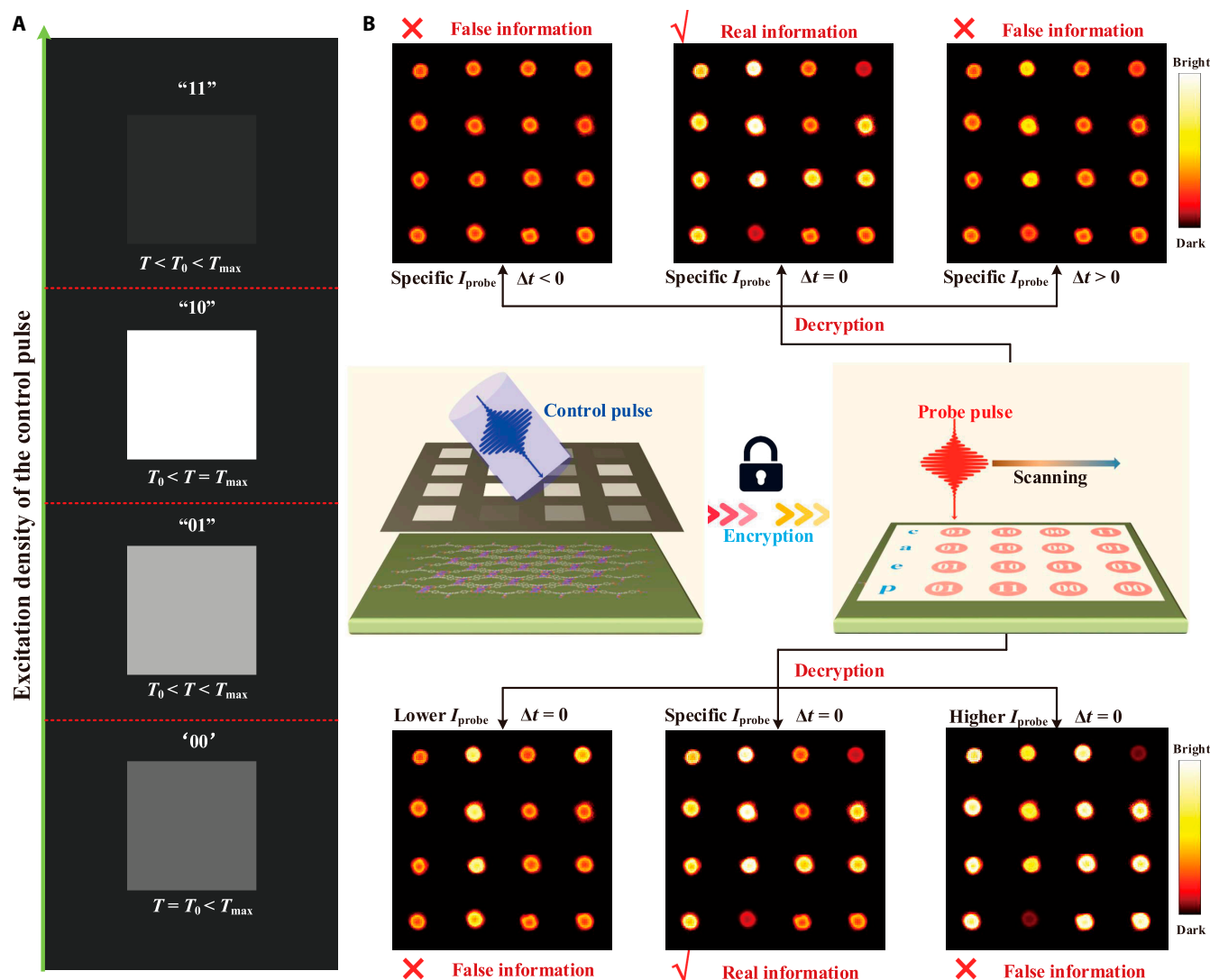


Fig. 4. Proof-of-concept demonstration of the ultrafast logic gates for optical encryption. (A) Schematic diagram of 4 probe transmittance states with the control pulse modulation, in which T_{max} denotes the probe transmittance with the strongest SA effect and T_0 denotes the probe transmittance without the control pulse. (B) Decryption of coded information by scanning the probe transmittance. The control pulse with a predesigned intensity pattern is exciting the SURMOF sample to encode 4 letters “caep.” The real information could only be acquired unless a probe pulse excited at $\Delta t = 0$ with a specific excitation intensity is adopted. Otherwise, the pattern is merely translated into meaningless information.

achieved at the transition excitation density from SA to RSA. According to the American Standard Code for Information Interchange binary codes, an arbitrary character can be translated into a standard 8-bit binary code sequence, e.g., “01100011” for the letter “c.” Therefore, specific raw information composed of several English characters, for instance, “caep” (acronym of China Academy of Engineering Physics), can be effectively translated into a 4×4 control–pulse–excitation array, where the excitation density ($I_{control}$) of an individual control–pulse–excitation spot in a specific position is determined according to the predesigned transmittance under a “reading” pulse (i.e., the probe pulse).

As a demo of our information encryption techniques, a 4×4 control–pulse–excitation array with predesigned $I_{control}$ distributions representing the coded information “caep” is illuminating the porphyrin-based SURMOF sample. Then, the coded information is decrypted by collecting the probe transmittance from every control–pulse–excitation spot in the whole array (see Fig. 4B). As mentioned above, since the probe transmittance

is closely dependent on I_{probe} and the time separation (Δt) between control/probe pulses, the security information could not be identified whatsoever with a random probe pulse excitation intensity (I_{probe}) or under a time-mismatched probe reading (i.e., $\Delta t \neq 0$). Here, based on our design, the probe pulse excited at $\Delta t = 0$ ps with a specific excitation density of 13.69 GW/cm^2 has to be used and the real information could be accurately acquired after evaluating the probe transmittance from individual control–pulse–excitation spots (see the “real information” subfigure in Fig. 4B). Otherwise, the pattern can merely be translated into meaningless information if the temporal overlapping requirement is not satisfied (see “false information” subfigures in the upper panel of Fig. 4B) or a random I_{probe} is adopted (see “false information” subfigures in the lower panel of Fig. 4B). These results show that the proposed information encryption technique based on ultrafast MOF-based optical logic gates significantly enhances the security of the information, exhibiting superiority in avoiding information leakage.

Conclusion

In summary, we have demonstrated that the nonlinear optical absorption process in porphyrin-based SURMOFs can be utilized to achieve all-optical logic gates with superior performances. On the basis of optical control-probe schemes with varied time ordering, Boolean logics with AND and XOR gates have been realized with an on-off ratio above 90% and an ultrafast speed approaching 1 THz. On this basis, we have further realized a novel quaternary coding platform and exhibited a proof-of-concept demonstration of cryptographic application with high security. We postulate that these results would provide valuable enlightenment to the novel design of MOF-based optoelectronic applications.

Acknowledgments

Funding: This work was supported by Science Challenge Project (no. TZ2018001), National Natural Science Foundation of China (nos. 11872058 and 21802036), Project of State Key Laboratory of Environment-friendly Energy Materials, and Southwest University of Science and Technology (21fksy07).
Competing interests: The authors declare that they have no competing interests.

Data Availability

The data are available from the authors upon a reasonable request.

Supplementary Materials

Figs. S1 to S8
 Note S1

References

- Maram R, Howe J, Kong D, Ros FD, Guan P, Galili M, Morandotti R, Oxenløwe LK, Azaña J. Frequency-domain ultrafast passive logic: NOT and XNOR gates. *Nat Commun.* 2020;11:5839.
- El Helou C, Buskohl PR, Tabor CE, Harne RL. Digital logic gates in soft, conductive mechanical metamaterials. *Nat Commun.* 2021;12:1633.
- Chien AA, Karamcheti V. Moore's law: The first ending and a new beginning. *Computer.* 2013;46:48–53.
- Ball P. Computer engineering: Feeling the heat. *Nature.* 2012;492:174–176.
- Markov IL. Limits on fundamental limits to computation. *Nature.* 2014;512:147–154.
- Feng J, Wang J, Fieramosca A, Bao R, Zhao J, Su R, Peng Y, Liew TCH, Sanvitto D, Xiong Q. All-optical switching based on interacting exciton polaritons in self-assembled perovskite microwires. *Sci Adv.* 2021;7:eabj6627.
- Cheng Y, Hong H, Zhao H, Wu C, Pan Y, Liu C, Zuo Y, Zhang Z, Xie J, Wang J, et al. Ultrafast optical modulation of harmonic generation in two-dimensional materials. *Nano Lett.* 2020;20:8053–8058.
- Willner AE, Khaleghi S, Chitgarha MR, Yilmaz OF. All-optical signal processing. *J Light Technol.* 2014;32:660–680.
- Fu Y, Hu X, Lu C, Yue S, Yang H, Gong Q. All-optical logic gates based on nanoscale plasmonic slot waveguides. *Nano Lett.* 2012;12:5784–5790.
- Miller DAB. Are optical transistors the logical next step? *Nat Photonics.* 2010;4:3–5.
- Yu J, Sharma M, Sharma A, Delikanli S, Volkan Demir H, Dang C. All-optical control of exciton flow in a colloidal quantum well complex. *Light Sci Appl.* 2020;9:27.
- Gu C, Zhang H, You P, Zhang Q, Luo G, Shen Q, Wang Z, Hu J. Giant and multistage nonlinear optical response in porphyrin-based surface-supported metal-organic framework nanofilms. *Nano Lett.* 2019;19:9095–9101.
- Tsai H, Shrestha S, Vilá RA, Huang W, Liu C, Hou CH, Huang HH, Wen X, Li M, Wiederrecht G, et al. Bright and stable light-emitting diodes made with perovskite nanocrystals stabilized in metal-organic frameworks. *Nat Photon.* 2021;15:843–849.
- Li D-J, Li QH, Wang ZR, Ma ZZ, Gu ZG, Zhang J. Interpenetrated metal-porphyrinic framework for enhanced nonlinear optical limiting. *J Am Chem Soc.* 2021;143:17162–17169.
- Gu C, Zhang H, Yu J, Shen Q, Luo G, Chen X, Xue P, Wang Z, Hu J. Assembled exciton dynamics in porphyrin metal-organic framework nanofilms. *Nano Lett.* 2021;21:1102–1107.
- Liu J, Wöll C. Surface-supported metal-organic framework thin films: Fabrication methods, applications, and challenges. *Chem Soc Rev.* 2017;46:5730–5770.
- Kalanoor BS, Gouda L, Gottesman R, Tirosh S, Haltzi E, Zaban A, Tischler YR. Third-order optical nonlinearities in organometallic methylammonium lead iodide perovskite thin films. *ACS Photonics.* 2016;3:361–370.
- Biswal BP, Valligatla S, Wang M, Banerjee T, Saad NA, Mariserla BMK, Chandrasekhar N, Becker D, Addicoat M, Senkovska I, et al. Nonlinear optical switching in regioregular porphyrin covalent organic frameworks. *Angew Chem Int Ed.* 2019;58:6896–6900.
- Gliemann H, Wöll C. Epitaxially grown metal-organic frameworks. *Mater Today.* 2012;15:110–116.
- Du M, Li Q, Zhao Y, Liu C-S, Pang H. A review of electrochemical energy storage behaviors based on pristine metal-organic frameworks and their composites. *Coord Chem Rev.* 2020;416:Article 213341.
- Zhu L, Liu X, Jiang H, Sun L. Metal-organic frameworks for heterogeneous basic catalysis. *Chem Rev.* 2017;117:8129–8176.
- Hirata S, Totani K, Yamashita T, Adachi C, Vacha M. Large reverse saturable absorption under weak continuous incoherent light. *Nat Mater.* 2014;13:938–946.
- Wang Z, Błaszczuk A, Fuhr O, Heissler S, Wöll C, Mayor M. Molecular weaving via surface-templated epitaxy of crystalline coordination networks. *Nat Commun.* 2017;8:14442.
- Gaur A, Syed H, Yendeti B, Soma VR. Experimental evidence of two-photon absorption and its saturation in malachite green oxalate: A femtosecond Z-scan study. *J Opt Soc Am B.* 2018;35(11):2906–2914.
- Guan M, Chen D, Hu S, Zhao H, You P, Meng S. Theoretical insights into ultrafast dynamics in quantum materials. *Ultrafast Sci.* 2022;2022:Article 9767251.
- Zhou Y-K, Li XZ, Zhou QN, Xing RH, Zhang Y, Bai B, Fang HH, Sun HB. Transient superdiffusion of energetic carriers in transition metal dichalcogenides visualized by ultrafast pump-probe microscopy. *Ultrafast Sci.* 2022;2022:0002.

27. Wang J, Hernandez Y, Lotya M, Coleman JN, Blau WJ. Broadband nonlinear optical response of graphene dispersions. *Adv Mater.* 2009;21:2430–2435.
28. Xu Y, Wang W, Ge Y, Guo H, Zhang X, Chen S, Deng Y, Lu Z, Zhang H. Stabilization of black phosphorous quantum dots in PMMA nanofiber film and broadband nonlinear optics and ultrafast photonics application. *Adv Funct Mater.* 2017;27:1702437.
29. Wang K, Wang J, Fan J, Lotya M, O'Neill A, Fox D, Feng Y, Zhang X, Jiang B, Zhao Q, et al. Ultrafast saturable absorption of two-dimensional MoS₂ nanosheets. *ACS Nano.* 2013;7:9260–9267.
30. Jiang X, Liu S, Liang W, Luo S, He Z, Ge Y, Wang H, Cao R, Zhang F, Wen Q, et al. Broadband nonlinear photonics in few-layer MXene Ti₃C₂T_x (T = F, O, or OH). *Laser Photonics Rev.* 2018;12:1700229.
31. Liu J, Zhou W, Liu J, Fujimori Y, Higashino T, Imahori H, Jiang X, Zhao J, Sakurai T, Hattori Y, et al. A new class of epitaxial porphyrin metal–organic framework thin films with extremely high photocarrier generation efficiency: Promising materials for all-solid-state solar cell. *J Mater Chem A.* 2016;4(33):12739–12747.
32. Goushi K, Yoshida K, Sato K, Adachi C. Organic light-emitting diodes employing efficient reverse intersystem crossing for triplet-to-singlet state conversion. *Nat Photon.* 2012;6:253–258.
33. Quan C, He M, He C, Huang Y, Zhu L, Yao Z, Xu X, Lu C, Xu X. Transition from saturable absorption to reverse saturable absorption in MoTe₂ nano-films with thickness and pump intensity. *Appl Surf Sci.* 2018;457:115–120.
34. Yu J, Shendre S, Koh WK, Liu B, Li M, Hou S, Hettiarachchi C, Delikanli S, Hernández-Martínez P, Birowosuto MD, et al. Electrically control amplified spontaneous emission in colloidal quantum dots. *Sci Adv.* 2019;5:Article eaav3140.
35. Yu J, Hou S, Sharma M, Tobing LYM, Song Z, Delikanli S, Hettiarachchi C, Zhang D, Fan W, Birowosuto MD, et al. Strong plasmon–Wannier Mott exciton interaction with high aspect ratio colloidal quantum wells. *Matter.* 2020;2:1550.
36. Kobayashi Y, Heide C, Kelardeh HK, Johnson A, Liu F, Heinz TF, Reis DA, Ghimire S. Polarization flipping of even-order harmonics in monolayer transition-metal dichalcogenides. *Ultrafast Sci.* 2021;2021:Article 9820716.
37. Zhang X, Wang M, Ma L, Fu Y, Guo J, Ma H, Zhang Y, Yan Z, Han X. Ultrafast two-photon optical switch using single crystal hybrid halide perovskites. *Optica.* 2021;8:735–742.
38. Wang K, Zhang W, Gao Z, Yan Y, Lin X, Dong H, Zhang C, Zhang W, Yao J, Zhao YS. Stimulated emission-controlled photonic transistor on a single organic triblock nanowire. *J Am Chem Soc.* 2018;140(41):13147–13150.
39. Yu J, Han Y, Zhang H, Ding X, Qiao L, Hu J. Excimer Formation in the non-van-der-Waals 2D semiconductor Bi₂O₂Se. *Adv Mater.* 2022;34:2204227.
40. Yu J, Sharma M, Li M, Delikanli S, Sharma A, Taimoor M, Altintas Y, McBride JR, Kusserow T, Sum TC, et al. Low-threshold lasing from copper-doped CdSe colloidal quantum wells. *Laser Photonics Rev.* 2021;15:2100034.